ChemistrySelect

Research Article
doi.org/10.1002/slct.202402091

Chemistry Europe
European Chemical Societies Publishing

www.chemistryselect.org

An Extensive Computational Investigation of *Mycobacterium tuberculosis* Pantothenate Synthetase Inhibitors from Diverse-Lib Compounds Library

Mohd Imran,[a] Abida,[a] Arbi Guetat,[b] Patrick Gad Iradukunda,[c] Shuaibu Abdullahi Hudu,[d] Eric Saramba,[c] Abdullah R. Alzahrani,[e] Lina Eltaib,[f] Mehnaz Kamal,[g] and Tafadzwa Dzinamarira*[h]

Antibiotics have played a crucial role in significantly reducing the incidence of tuberculosis (TB) infection worldwide. Even before the mid-20th century, the mortality rate of TB onset within five years was around 50%. So, the introduction of antibiotics has changed the scenario of TB from a serious threat to a manageable one. However, the emergence of resistance to anti-TB drugs poses a significant challenge. So, to overcome this situation the therapeutic approaches and drug targets need to be reformed. This study focused on finding potential inhibitors by targeting Pantothenate Synthetase, a crucial enzyme for *Mycobacterium tuberculosis* (Mtb) survival, through computational drug discovery methods. Molecular docking and virtual screening were employed to identify potential inhibitors from Diverse-lib. Four compounds, namely CID2813602, 24357538, CID753354, and CID4798023, exhibited strong binding energies and stable interaction with the target protein. Further assessment of these compounds through MD simulation and Post MD simulation showed significant dynamic stability. The minimum energy transition calculated using the free energy landscape analysis of these compounds when docked with Pantothenate Synthetase confirmed the stability of each complex due to its minimum energy production. The free binding energy calculation of each complex also showed the intramolecular interaction contributes to the strong binding affinity of the compounds within the enzyme's active site clarifying their mechanisms of action. This research showcases the effectiveness of computational methods in promptly identifying potential anti-TB drugs, paving the way for future experimental validation and optimization. It holds promise for the development of new treatments targeting drug-resistant TB strains.

1. Introduction

Tuberculosis (TB), caused by the *Mycobacterium tuberculosis* (*Mtb*), remains one of the most challenging infectious diseases, impacting millions worldwide.[11] It is the leading cause of death due to a single infectious agent, surpassing even HIV/AIDS.[21] The disease primarily affects the lungs, but can also damage other parts of the body.[26] Despite significant efforts in controlling TB, the emergence of drug-resistant strains, coupled with the complexities of long-term antibiotic treatments, presents ongoing challenges.[16] *Mtb* has a complex and unique biology. It's a slow-growing bacterium with a thick, waxy cell wall, contributing to its resistance against both the immune responses of the host and many antibiotics.[6] This resilience underscores the necessity for novel therapeutic strategies. Researchers have identified several potential targets within the bacterium's metabolic pathways, essential for its survival and virulence.[32] One such target is the enzyme Pantothenate Synthetase (PS).[39]

[a] *M. Imran, Abida*
Department of Pharmaceutical Chemistry, College of Pharmacy, Northern Border University, Rafha 91911, Saudi Arabia

[b] *A. Guetat*
Department of Biological Sciences, College of Sciences, Northern Border University, Arar 73213, Saudi Arabia

[c] *P. G. Iradukunda, E. Saramba*
University of Rwanda, Kigali, Rwanda

[d] *S. A. Hudu*
Department of Basic Medical and Dental Sciences, Faculty of Dentistry, Zarqa University, Jordan

[e] *A. R. Alzahrani*
Department of Pharmacology and Toxicology, Faculty of Medicine, Umm Al-Qura University, Al-Abidiyah, P.O. Box 13578, Makkah, 21955, Saudi Arabia

[f] *L. Eltaib*
Department of Pharmaceutics, College of Pharmacy, Northern Border University, Rafha 91911, Saudi Arabia

[g] *M. Kamal*
Department of Pharmaceutical Chemistry, College of Pharmacy, Prince Sattam Bin Abdulaziz University, Al-Kharj 11942, Saudi Arabia

[h] *T. Dzinamarira*
School of Health Systems and Public Health, University of Pretoria, Pretoria, South Africa
E-mail: u19395419@up.ac.za

Supporting information for this article is available on the WWW under https://doi.org/10.1002/slct.202402091

Recent research has focused on Pantothenate Synthetase as a novel target for therapeutic intervention.[18] PS plays a critical role in the biosynthesis of Coenzyme A (CoA) in *Mtb*.[3] CoA is vital for various metabolic processes, including fatty acid synthesis and energy production, crucial for the bacterium's survival and pathogenicity.[7] Targeting PanC could potentially disrupt the metabolic functions critical for bacterial growth and survival. Studies have shown that inhibitors of PanC exhibit substantial activity against drug-resistant TB strains, highlighting the enzyme's potential as a therapeutic target. This makes PS an attractive target for new anti-TB drugs.[10,35] In comparison, other validated targets, such as InhA (enoyl-ACP reductase) and DprE1 (decaprenylphosphoryl-β-D-ribose 2′-epimerase), also exhibit high essentiality due to their involvement in vital metabolic and cell wall biosynthesis pathways. Pantothenate Synthetase has a well-defined active site amenable to small-molecule binding, as evidenced by the successful identification of several potent inhibitors through structure-based drug design.[36] The enzyme's active site provides numerous interaction points for potential inhibitors, enhancing its druggability. In comparison, targets like InhA and DprE1 are also considered highly druggable, having been the focus of extensive drug development efforts that yielded effective inhibitors.

However, drug development against TB, particularly targeting PS, is not straightforward. The challenge lies in identifying compounds that are not only effective in inhibiting the target enzyme but also possess favorable pharmacokinetic properties and minimal toxicity.[29] The traditional drug discovery process is often time-consuming and costly, with a high rate of attrition.[12] This is where computational drug discovery methods come into play. These approaches can significantly accelerate the drug discovery process, enabling the identification of potential drug candidates more efficiently and cost-effectively.[14,38]

In this context, the Diverse-lib Compounds library available at the MTiOpenScreen database presents a valuable resource. This library is a curated collection of compounds with potential therapeutic properties, encompassing a wide range of chemical structures.[17,22] The availability of such a diverse library is instrumental in broadening the scope of virtual screening endeavours, increasing the likelihood of identifying novel inhibitors.

Our work leverages the Diverse-lib Compounds library to identify potential inhibitors of Pantothenate Synthetase from *Mtb*. We employed a computational drug discovery approach, integrating virtual screening with Lipinski's filter to ensure the selection of Diverse-lib compounds. This was followed by re-docking studies to refine our understanding of the binding interactions. Furthermore, the integration of molecular dynamics simulations and binding free energy calculations provides a deeper understanding of the molecular interactions and stability of potential inhibitors. This helps in refining the selection and optimization of compounds, ensuring they not only bind effectively to the target but also possess favorable pharmacokinetic and pharmacodynamic properties. By doing so, we aim to contribute to the global effort in combating tuberculosis and address the growing challenge of drug resistance. The findings represent a stride towards the discovery of new, effective treatments that can potentially save millions of lives affected by this devastating disease.

Methodology

Protein Structure Data Collection

Our study commenced with the collection of the protein structure data for Pantothenate Synthetase (PS), a crucial enzyme in *Mtb*. The crystal structure of PS (PDB ID: 1 N2H) was obtained from the Protein Data Bank (PDB), a widely recognized repository for 3D structural data of proteins and nucleic acids.[2,35] The structure was then meticulously cleaned by removing extraneous molecules like water and ions. Subsequently, we optimized it by adding missing hydrogen atoms and correcting any structural anomalies. This prepared PS structure was then used to initiate computational analysis, including virtual screening and re-docking simulations.

Virtual Screening Using MTiOpenScreen and Drug-Lib Compounds

The virtual screening process was conducted using the MTiOpenScreen webserver, a powerful tool for identifying potential inhibitors from large compound libraries.[17] We utilized the Diverse-lib Compounds database, a curated collection of 3D conformations of 99,288 diverse, drug-like compounds, as our primary source. Each compound from this database was screened against the PS protein to predict their binding affinity and interaction. The MTiOpenScreen webserverfacilitated this process by employing advanced algorithms to simulate the docking of each compound to the protein, providing us with a ranked list of potential inhibitors based on their predicted binding affinities.[17] The process involved the careful positioning of each compound in the active site of PS, which was identified as the grid centre (X = 31.93, Y = 34.34 and Z = 43.0). The grid box size (20X20X20 Å) was determined based on the position of the pre-bound ligand observed in the crystal structure of PS. This approach allowed for precise and realistic simulation of the compound-enzyme interactions, providing us with detailed insights into the binding mechanisms and the stability of each compound within the active site.

Re-Docking Using AutoDock Vina Chimera Plugin

To further refine our results and validate the binding modes of the 4 top-ranked compounds from the virtual screening, we performed re-docking simulations. The re-docking process was meticulously executed using AutoDock Vina within the Chimera interface, ensuring a high degree of accuracy and consistency with the initial virtual screening.[9,24] Crucially, we maintained the same grid center and box size parameters for re-docking as used in the virtual screening phase. This consistency was pivotal in ensuring that any observed differences in ligand binding interactions were attributable to the intrinsic properties of the ligands, rather than alterations in the docking environment. The AutoDock Vina plugin facilitated a precise repositioning of each ligand in the active site of Pantothenate Synthetase, allowing us to closely observe and analyze the binding affinity and interaction patterns. This process was crucial for validating the results from the virtual screening and for gaining deeper insights into the molecular interactions, thereby enhancing the reliability of our findings in identifying potential inhibitors.

Molecular Dynamics (MD) Simulation

To investigate the dynamic behavior and stability of our selected 1 N2H inhibitors, we conducted molecular dynamics (MD) simulations using the AMBER software suite.[4,5] Our study included three 1 N2H-ligand complexes, identified from the Diverse-lib database, as well as a control system comprising the 1 N2H protein without any bound ligand.[17,22]

System Preparation

For all MD simulations, we utilized the Generalized Amber Force Field (GAFF).[34] Ligand parameters were generated using the Antechamber module in AMBER,[33] ensuring accurate representation of atomic charges and topologies. Each ligand was parametrized individually before integration into the respective protein complexes. The 1 N2H protein structure was prepared by removing any water molecules and ions from the crystal structure. The LEaP module of AMBER was employed to combine the 1 N2H protein and the ligands, creating the 1 N2H-ligand complexes.[4] Each complex was then solvated in a rectangular box using the TIP3P water model, extending 10 Å from the solute, ensuring adequate solvation and minimizing boundary effects. Counterions were added to neutralize the system.[19]

Minimization and Equilibration

Each system underwent a two-step energy minimization process to relieve any steric clashes or unfavorable interactions. Initially, the solute atoms were restrained, allowing the solvent molecules to relax. Subsequently, the entire system was minimized without restraints. Following minimization, the systems were gradually heated from 0 K–300 K over 50 ps using the NVT ensemble, applying harmonic restraints on the solute. Equilibration was performed in two phases: first, 1 ns of constant volume equilibration (NVT), followed by 1 ns of constant pressure equilibration (NPT) at 1 atm. Harmonic restraints on the solute were gradually reduced during these phases. The Particle Mesh Ewald (PME) method was used to handle long-range electrostatics,[23] and the SHAKE algorithm constrained all hydrogen-containing bonds, allowing for a 2 fs time step.[27]

Production MD

Each equilibrated system was subjected to a 200 ns production MD run under NPT conditions, maintaining a constant temperature of 300 K and pressure of 1 atm. Trajectories were recorded every 2 ps for subsequent analysis.

Trajectory Analysis

Post-simulation, the trajectories were analyzed to assess the stability and conformational dynamics of the 1 N2H-ligand complexes. Root Mean Square Deviation (RMSD) and Root Mean Square Fluctuation (RMSF) analyses were conducted to evaluate the structural stability and flexibility of the protein residues, respectively. Additionally, the radius of gyration (RG) was calculated to monitor the compactness of the protein over time. Hydrogen bond analysis was performed to examine the persistence and patterns of interactions between the 1 N2H protein and the ligands. The MM-GBSA method was employed to estimate the binding free energies, providing insights into the binding affinity of each ligand.

MM-GBSA Calculations

We calculated the binding free energy (MM-GBSA) of the protein-ligand complexes from MD simulation trajectories using the MMPBSA.py program, a component of the AmberTools23 package.[20] After completing MD simulations with AMBER, we extracted trajectories of protein-ligand complexes and selected representative snapshots based on stability, as indicated by RMSD and RMSF analyses. MMPBSA.py was then employed to calculate the binding free energy for each snapshot. This program computes the molecular mechanic's energies (electrostatic and van der Waals interactions), solvation free energy (including polar and nonpolar components), and an estimation of the entropic contributions. By averaging these values across all snapshots, we obtained a comprehensive measure of the ligand's binding affinity to Pantothenate Synthetase. This approach provided us with a quantitative assessment, essential for determining the binding efficacy of the ligands and identifying the most promising candidates as potential inhibitors of *Mtb.*

PCA-Based Free Energy Landscape, Structure Extraction, and Superimposition

We implemented a comprehensive approach for analyzing the PCA-based free energy landscape and the subsequent extraction and superimposition of minima structures. Initially, Principal Component Analysis (PCA) was performed on the molecular dynamics (MD) simulation trajectories using the Geo Measures PyMOL Plugin.[8,15] This step was crucial for reducing the dimensionality of the data and concentrating on the most significant movements within the protein-ligand complexes. We focused on the first two principal components, which generally capture the majority of the system's variance, to construct the free energy landscape. This landscape provided insights into the conformational stability and transition states of the complexes. Following this, we extracted the minima structures from these landscapes using Visual Molecular Dynamics (VMD) software.[13] These structures represent the most stable conformations of the complexes within the simulated environment. Finally, for a detailed comparative analysis, these minima structures were superimposed using the Chimera software.[24] This allowed us to visually assess and compare the conformational changes and the binding modes of the ligands in the active site of Pantothenate Synthetase, offering valuable insights for the identification of potent inhibitors against *Mtb.*

2. Results

2.1. Virtual Screening Analysis

Virtual screening is an essential computer-based approach to finding lead compounds from a large database. A comprehensive analysis of 99,288 compounds from a diverse-lib of compounds was carried out using the Lipinski filter. Thus, 1,500 compounds have been identified and they are shown in supplementary Table S1 with binding scores ranging from −11.3 kcal/mol−−9 kcal/mol. Due to the high binding scores of −11.3 kcal/mol, −11.3 kcal/mol, −11.2 kcal/mol, and −11.2 kcal/mol, respectively, four compounds identified as CID2813602, CID6622018, CID753354, and CID4798023 (CIDs of these Diverse-lib compounds were accessed from Diverse-lib using their structures) were selected for further studies (supplementary Table S2).

2.2. Re-Docking and Intermolecular Analysis

Re-docking has become an essential approach in therapeutic research, involving a thorough reassessment of the interaction between ligand and receptor molecules. In this study, selected ligands were subjected to a re-docking procedure against the target protein PS, in parallel with a reference molecule. This selection was guided by the intent to assess the stability and binding affinity of the protein PS with the ligand in question. The binding energies, of PS_CID2813602, PS_24357538, PS_CID753354, and PS_CID4798023 were −10.9 kcal/mol, −11.4 kcal/mol, −11.3 kcal/mol, and −10.2 kcal/mol, respectively. As depicted in Figure 1 the 3D structure of each complex was created using PyMOL.[30] Additionally, a reference molecule, Pantoyl Adenylate (PA), was selected for further investigation due to its low binding energy, which was also re-docked in the same binding site of the target protein and the re-docking score obtained was −9.6 Kcal/mol. In comparison, the known

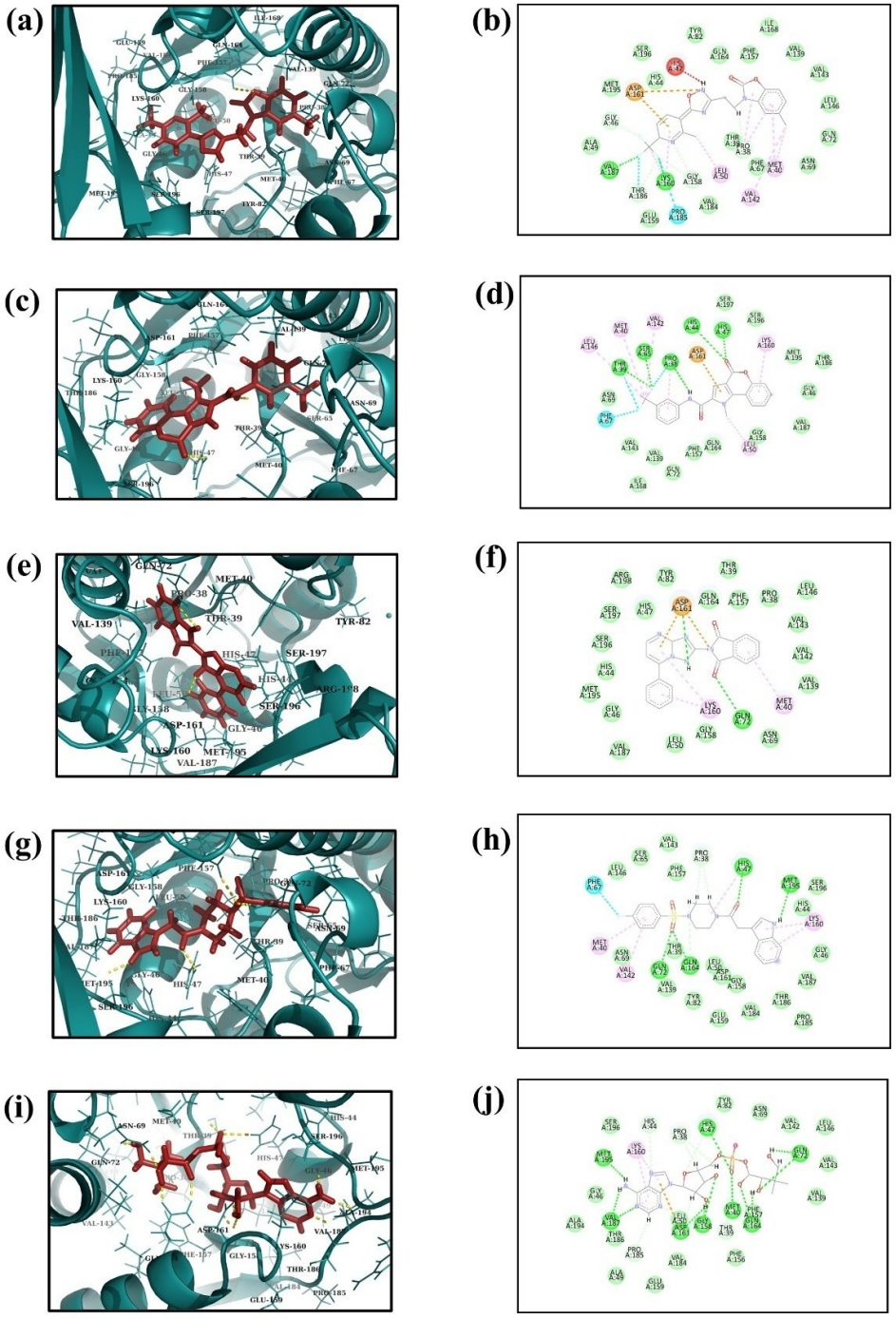

Figure 1. 3D and 2D interaction of four selected compounds (a–b) PS_CID2813602, (c–d) PS_24357538, (e–f) PS_CID753354, (g–h) PS_CID4798023 and the control complex (i–j) PS_PA docked with the targeted protein.

inhibitors of other essential M. tuberculosis enzymes, such as InhA and Pks13, generally exhibit binding energies of −9.8 and −10.3 kcal/mol.[1] The evaluated compounds show competitive binding affinities, suggesting their potential as effective inhibitors and highlighting their promise for further development in combating drug-resistant TB. The ADMET analysis of the five compounds (CID2813602, CID24357538, CID753354, CID4798023, and a control compound) reveals several promising attributes across their pharmacokinetic and safety profiles, suggesting strong potential for further development and optimization. CID2813602 demonstrates moderate absorption and distribution, indicating effective systemic circulation, with high plasma protein binding (PPB) contributing to prolonged therapeutic effects. Its interactions with CYP (Cytochrome P450) enzymes provide opportunities for fine-tuning to enhance bioavailability. CID24357538, despite its lower solubility and permeability, shows significant CYP enzyme interactions, which can be strategically modified to improve absorption and therapeutic efficacy. CID753354 stands out with excellent absorption and an extended half-life, ideal for sustained therapeutic action, reducing the need for frequent dosing. CID4798023 is notable for its exceptional blood-brain barrier penetration, making it a strong candidate for central nervous system applications, with its high clearance rate ensuring efficient elimination and reduced toxicity. The control compound exhibits a well-balanced ADMET profile, with low CYP interactions, good solubility, and reduced carcinogenic potential, suggesting a lower risk of adverse interactions and a favorable safety profile. These findings highlight the unique strengths of each compound, demonstrating their potential for therapeutic development. With targeted optimization to enhance bioavailability and minimize toxicity, these compounds can be refined into effective and safe therapeutic agents, underscoring the value of ADMET profiling in guiding successful drug development.

We have also performed the ADMET analysis to predict the safety and toxicity of the selected compounds as shown in Table S2.

As shown in Figure 1 the 2D structure was generated by Biodiscovery Studio.[28] Compound CID2813602 in Complex PS_CID2813602 demonstrated a significant variety of interactions. Primarily, it formed a hydrogen bond with the Lys^{160}, and Val^{187} residue, which is indicative of a potential key anchoring point within the binding site. Furthermore, it engages in seventeen hydrophobic interactions with a range of residues, including Thr^{39}, His^{44}, Ala^{49}, Phe^{67}, Asn^{69}, Gln^{72}, Tyr^{82}, Val^{139}, Val^{143}, Leu^{146}, Phe^{157}, Glu^{159}, Gln^{164}, Ile^{168}, Val^{184}, $Met^{195,}$ and Ser^{196}. These hydrophobic interactions likely contribute to the stabilization of the compound in complex with protein. Additionally, three pi-alkyl bonds are observed with residues Met^{40}, Leu^{50}, and Val^{142}, further enhancing the binding affinity. Compound 24357538 in Complex PS_24357538 exhibited the five-hydrogen bond with Pro^{38}, Thr^{39}, His^{44}, His^{47}, and Ser^{65}. It also shows fourteen hydrophobic interactions with residues including Gly^{46}, Asn^{69}, Gln^{72}, Val^{139}, Val^{143}, Phe^{157}, Gly^{158}, Gln^{164}, Ile^{168}, Thr^{186}, Val^{187}, Met^{195}, Ser^{196}, and Ser^{197} which contributes to its binding stability. Additionally, five pi-alkyl bonds with Met^{40}, Val^{142}, Leu^{146}, and Lys^{160} were observed. Compound CID753354 in Complex PS_CID753354 exhibited two pi-alkyl bonds with residues including Met^{40}, and Lys^{160}. Alongside these, twenty hydrophobic interactions are noted with residues Pro^{38}, Thr^{39}, His^{44}, Gly^{46}, His^{47}, Leu^{50}, Asn^{69}, Tyr^{82}, Val^{139}, Val^{142}, Val^{143}, Leu^{146}, Phe^{157}, Gly^{158}, Gln^{164}, Val^{187}, Met^{195}, Ser^{196}, Ser^{197}, and Arg^{198}. Compound CID4798023 in Complex PS_CID4798023 exhibited the six-hydrogen bond with Met^{40}, His^{47}, Gln^{72}, Gly^{158}, Asp^{161}, and Gln^{164}. It also shows nineteen hydrophobic interactions with residues including Thr^{39}, His^{44}, Gly^{46}, Leu^{50}, Ser^{65}, Asn^{69}, Asn^{69}, Val^{139}, Val^{143}, Leu^{156}, Phe^{157}, $Gly^{158,}$ Glu^{159}, Asp^{161}, Val^{184}, Pro^{185}, Thr^{186}, Val^{187}, and Ser^{19}. Additionally, three pi-alkyl bonds are also seen with residues Met^{40}, Val^{142}, and Lys^{160}. In the control complex, six hydrogen bonds are observed with the residue Met^{40}, His^{47}, Gln^{72}, Gly^{158}, Asp^{161}, and Gln^{164}. Seventeen hydrophobic interactions are present with residues including Gly^{46}, Ala^{49}, Leu^{50}, Asn^{69}, Asn^{69}, Tyr^{82}, Val^{139}, Val^{142}, Val^{143}, Leu^{146}, Leu^{156}, Phe^{157}, Glu^{159}, Val^{184}, Thr^{186}, Ala^{194}, and Ser^{196}.Additionally, single pi-alkyl bonds are also seen with residues Lys^{160} as shown in Table 1.

2.3. Molecular Dynamic Simulation

In the conducted research, the structural constancy and adaptability of the top four hit complexes were analyzed

Table 1. Intermolecular interaction of four complexes (a) PS_CID2813602, (b) PS_24357538, (c) PS_CID753354 (d) PS_CID4798023 and (e) control (PA) docked with the PS protein.

S no.	Complex	H-Bond	Hydrophobic	π-π stacking/π-π cation*
a	1 N2H CID2813602	A: Lys^{160}, Val^{187}	A: Thr^{39}, His^{44}, Ala^{49}, Phe^{67}, Asn^{69}, Gln^{72}, Tyr^{82}, Val^{139}, Val^{143}, Leu^{146}, Phe^{157}, Glu^{159}, Gln^{164}, Ile^{168}, Val^{184}, Met^{195}, Ser^{196}	A: Met^{40}, Leu^{50}, Val^{142}
b	1 N2H CID24357538	A: Pro^{38}, Thr^{39}, His^{44}, His^{47}, Ser^{65}	A: Gly^{46}, Asn^{69}, Gln^{72}, Val^{139}, Val^{143}, Phe^{157}, Gly^{158}, Gln^{164}, Ile^{168}, Thr^{186}, Val^{187}, Met^{195}, Ser^{196}, Ser^{197}	A: Met^{40}, Leu^{50}, Val^{142}, Leu^{146}, Lys^{160}
c	1 N2H CID753354	A: Gln^{72}	A: Pro^{38}, Thr^{39}, His^{44}, Gly^{46}, His^{47}, Leu^{50}, Asn^{69}, Tyr^{82}, Val^{139}, Val^{142}, Val^{143}, Leu^{146}, Phe^{157}, Gly^{158}, Gln^{164}, Val^{187}, Met^{195}, Ser^{196}, Ser^{197}, Arg^{198}	A: Met^{40}, Lys^{160}
d	1 N2H CID 4798023	A: His^{47}, Gln^{72}, Gln^{164}, Met^{195}	A: Thr^{39}, His^{44}, Gly^{46}, Leu^{50}, Ser^{65}, Asn^{69}, Asn^{69}, Val^{139}, Val^{143}, Leu^{156}, Phe^{157}, $Gly^{158,}$ Glu^{159}, Asp^{161}, Val^{184}, Pro^{185}, Thr^{186}, Val^{187}, Ser^{196}	A: Met^{40}, Val^{142}, Lys^{160}
e	PS_PA (Control)	A: Met^{40}, His^{47}, Gln^{72}, Gly^{158}, Asp^{161}, Gln^{164}	A: Gly^{46}, Ala^{49}, Leu^{50}, Asn^{69}, Asn^{69}, Tyr^{82}, Val^{139}, Val^{142}, Val^{143}, Leu^{146}, Leu^{156}, Phe^{157}, Glu^{159}, Val^{184}, Thr^{186}, Ala^{194}, Ser^{196}	A: Lys^{160}

utilizing 200 ns Molecular Dynamics (MD) simulations. These simulations played a pivotal role in evaluating the dynamic interactions within the complexes. Critical parameters such as Root Mean Square Deviation (RMSD) and Root Mean Square Fluctuation (RMSF) were thoroughly monitored for both the protein and ligand constituents. RMSD evaluations offered an understanding of the overall structural integrity, illustrating the variances in complex configurations from their initial states over time. Concurrently, RMSF assessments provided insights into the flexibility of individual amino acid residues, identifying regions of conformational variability that might influence ligand interaction. Furthermore, the analysis of hydrogen bond formation and its sustainability within each complex was conducted throughout the simulation, thereby enhancing comprehension of the intermolecular forces contributing to the stability of the complexes. This extensive analysis of RMSD, RMSF, and hydrogen bond dynamics has imparted significant knowledge about the dynamic characteristics and potential binding efficiency of these complexes, pivotal for advancing pharmacological research.

2.3.1. RMSD and RMSF Analysis

To investigate the dynamic behaviour and structural characteristics of four chemicals when attached to the target protein, a molecular dynamics (MD) simulation was run. The stability, interactions, and conformational changes within the system of the protein-ligand complexes were all well understood by this simulation. The stability of the protein-ligand complexes during the 200 ns simulation was assessed using the RMSD analysis. A comprehensive analysis of several complexes was done for the protein component as shown in Figure 2.

For complex PS_CID2813602, the ligand RMSD exhibited initial fluctuations, ranging from 2 Å–6 Å during the first 50 (ns) of the simulation. This variability suggests an initial period of adjustment as the ligand explores different conformations within the binding pocket of the protein. Following this period, the ligand attained a stable configuration, as evidenced by a consistent RMSD value for the remainder of the simulation. This stability indicates a well-established interaction between the ligand and the protein. Conversely, the protein RMSD in this complex showed stability (2 Å), implying that the protein structure did not undergo significant conformational during the simulation.

In complex PS_24357538, the ligand RMSD displayed notable fluctuations of approximately 4 Å till the end of 200 ns simulation. This level of deviation suggests a minor degree of conformational flexibility or instability in the ligand's interaction with the protein. Post this period, the ligand RMSD stabilized but continued to show considerable deviations. The protein RMSD for this complex was observed to be around 2 Å, indicating a relatively stable protein structure despite the ligand's fluctuations. Complex PS_CID753354 demonstrated a behaviour related to a reference molecule, with both the protein and ligand RMSDs achieving stable conformations. The protein RMSD maintained a steady state, suggesting minimal conformational changes in the protein structure throughout the simulation. The ligand RMSD in this complex was consistently within a stable range of 3 Å, indicating a reliable and stable interaction with the protein, comparable to the reference molecule. For complex PS_CID 4798023, the protein RMSD was characterized by a stable nature throughout the simulation. This indicates a dynamically stable protein structure. The ligand in this complex showed RMSD values below 2 Å, with insignificant deviations, suggesting a rigid interaction with the protein while maintaining an overall stable binding.

Comparatively, about the PA complex, compounds c and d exhibited similar RMSD patterns, implying a comparable level of stability in protein-ligand interactions. This consistency in RMSD values, especially in comparison with a known reference, provides valuable insights into the dynamic stability and reliability of the interactions within these complexes. Overall, the RMSD values from these MD simulations offer critical insights into the dynamic behaviours of protein-ligand interactions, highlighting the varying degrees of stability, that occur within these molecular complexes during the simulations. Such detailed analysis is crucial for understanding the molecular basis of protein-ligand binding and for guiding the development of potential therapeutic agents.

The quantification of root-mean-square fluctuation (RMSF) plays a pivotal role in elucidating the dynamic properties and conformational flexibility of protein structures. This study focused on the comparative analysis of RMSF values among four selected compounds as shown in Figure 3, namely PS_CID2813602, PS_24357538, PS_CID753354, and PS_CID 4798023. RMSF serves as a measure of the extent to which the atoms of a protein oscillate around their average positions. The investigation revealed that each of the four compounds exhibited RMSF values less than 3(Å), signifying relatively low amplitude fluctuations. In contrast, the RMSF value for the control complex was observed to be less than 4 Å, indicating a comparatively higher degree of atomic fluctuation. This differential in RMSF values is indicative of the variances in the dynamic behavior and structural flexibility between the compounds under study and the control complex.

2.3.1.1. RG Value Analysis

In the detailed scientific investigation of the molecular complexes, we examined the radius of gyration (Rg), a parameter that provides vital information about the size and shape of molecules in a solution as shown in Figure 4. Complex PS_CID2813602 exhibited an Rg value of less than 2.04 angstroms (Å), however, the measurements were characterized by some degree of fluctuation. These fluctuations potentially indicate a dynamic structural nature or conformational versatility within the complex, suggesting that the molecular arrangement may vary under different conditions or states. Complex PS_24357538 in contrast to PS_CID2813602, complex PS_24357538 displayed an RG value that exceeded 2.04 Å. This higher Rg value is indicative of a more expanded molecular structure, suggesting a different spatial arrangement or greater molecular extension

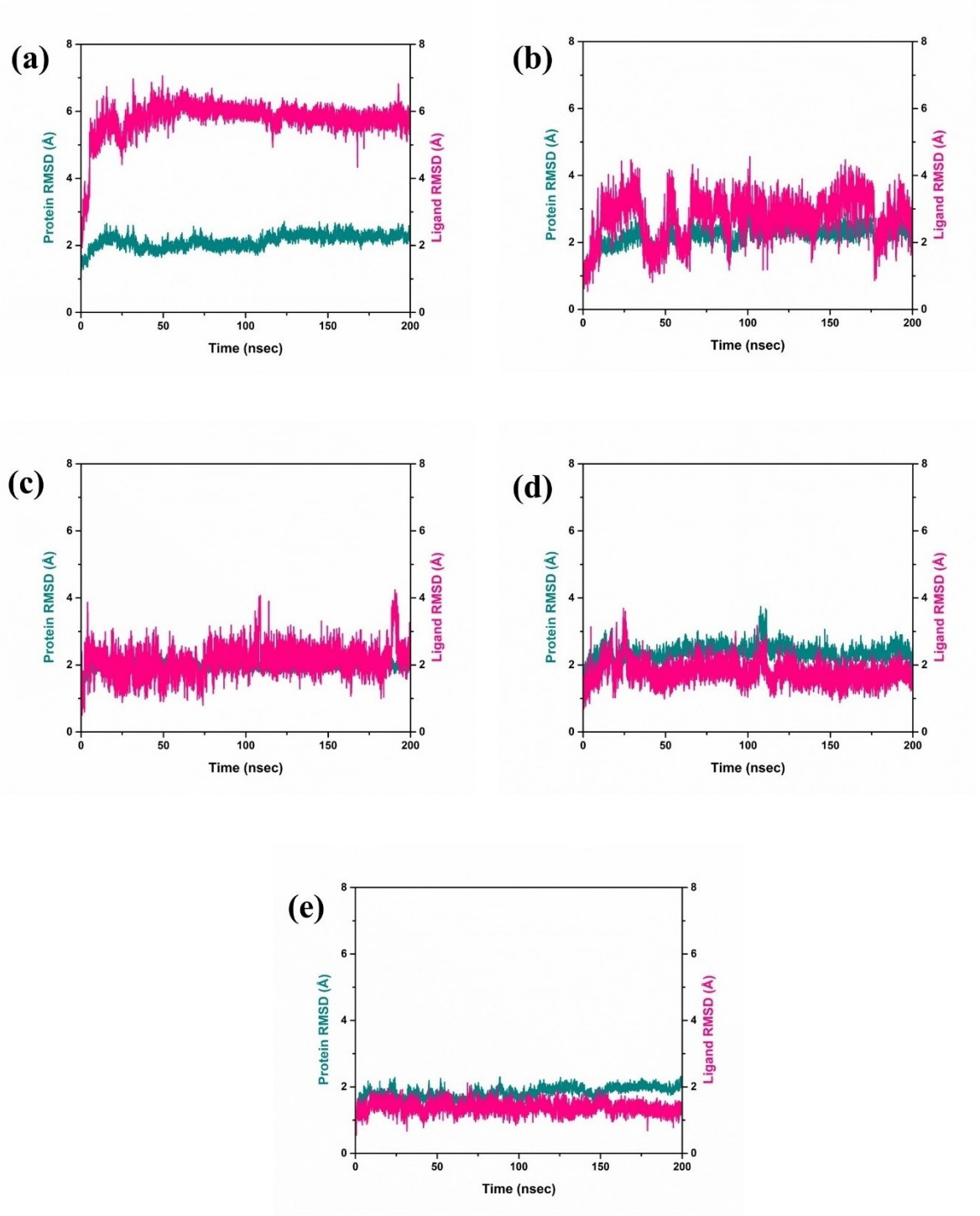

Figure 2. RMSD graph of four selected complexes (a) PS_CID2813602, (b) PS_24357538, (c) PS_CID753354 (d) PS_CID4798023 and (e) control (PA) docked with the PS protein.

relative to PS_CID2813602. While the complex PS_CID753354 exhibited RG value of less than 2.04 Å was recorded, aligning it closely with the structural characteristics observed in PS_CID2813602. This similarity in RG values suggests comparable molecular compactness or a related conformational profile. A distinct observation was made for complex PS_CID 4798023, where the RG value was greater than 2.04 Å but less than 2.06 Å. This range places the complex in an intermediate structural category, suggesting a conformation that is neither as compact as PS_CID2813602 and PS_CID753354 nor as expanded as PS_24357538. The control complex presented an RG value of less than 2.02 Å, marking it as the most compact structure among the analyzed samples. This lower RG value

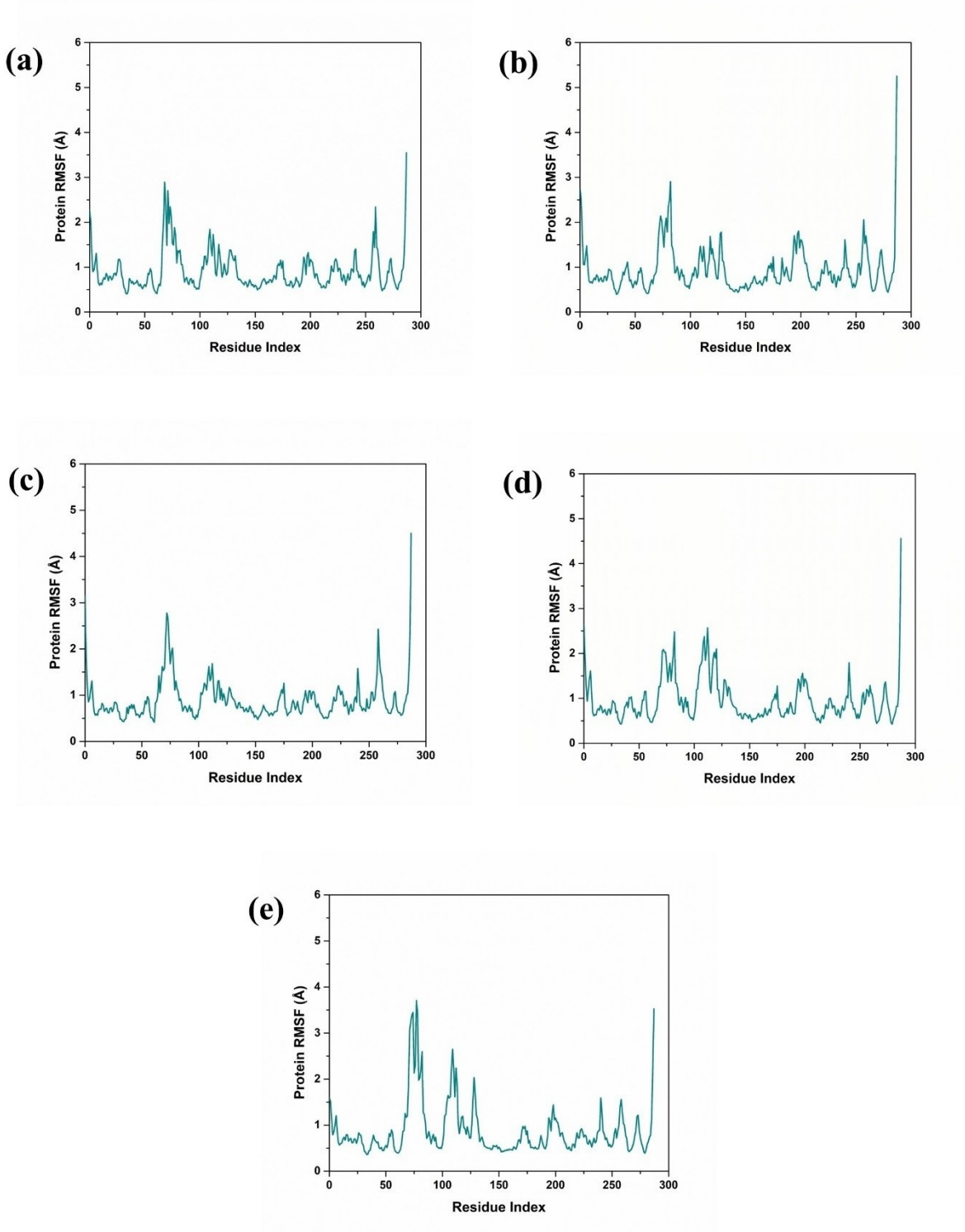

Figure 3. RMSF graph of four selected complexes (a) PS_CID2813602, (b) PS_24357538, (c) PS_CID753354 (d) PS_CID4798023 and (e) control (PA) docked with the PS protein.

provides a critical baseline for comparison, indicating a tighter molecular arrangement in comparison to the other complexes.

These RG values provide crucial insights into the extendedness of ligands in each complex, which are essential for understanding their behaviour and properties in solution. Such data are invaluable in fields like protein science, where RG can influence functional dynamics, and in nanotechnology, where molecular arrangement dictates material properties.

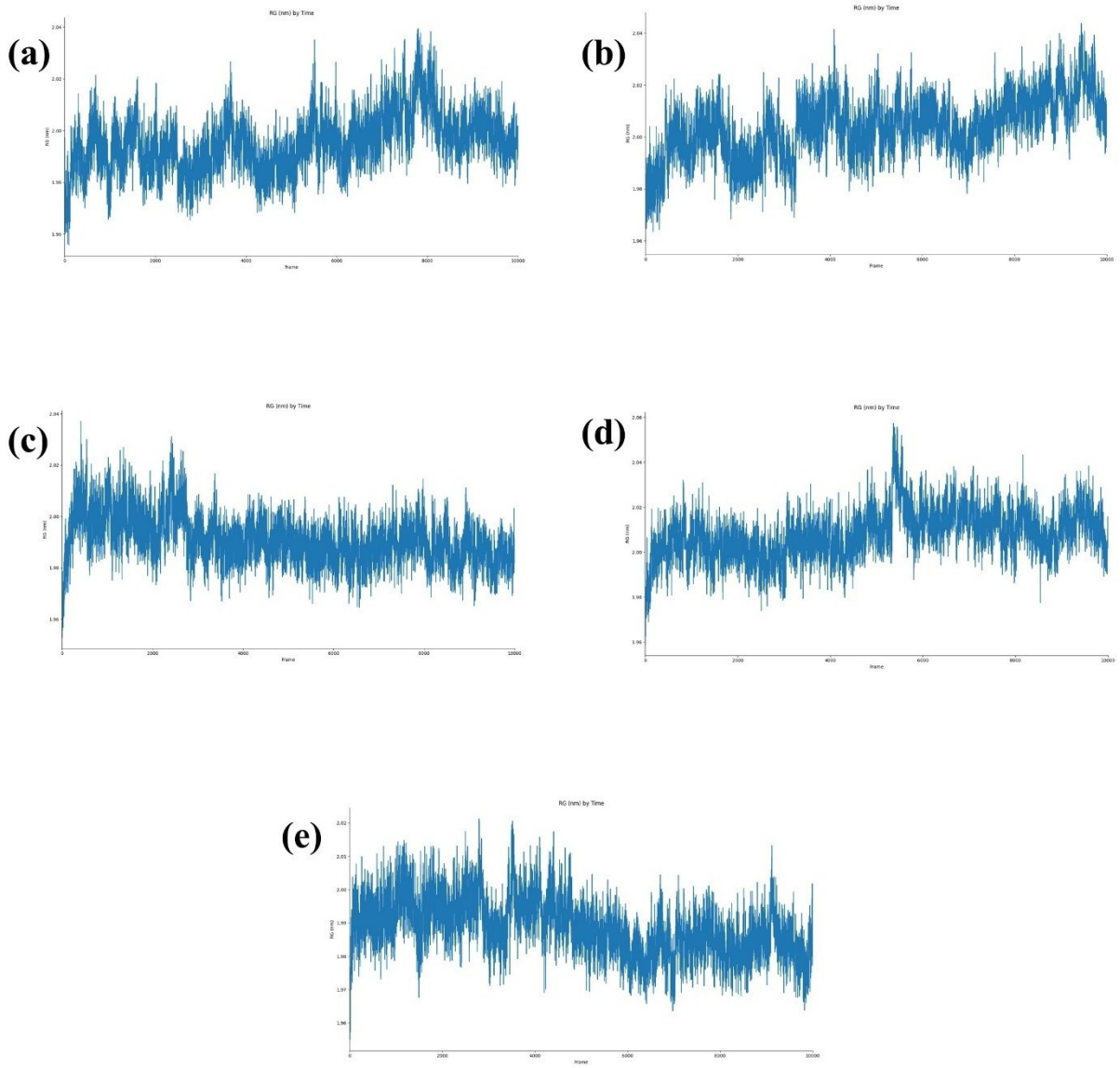

Figure 4. RG graph of four selected complexes (a) PS_CID2813602, (b) PS_24357538, (c) PS_CID753354 (d) PS_CID4798023 and (e) control (PA) docked with the PS protein.

2.3.2. Hydrogen Bond Analysis

In the molecular dynamics simulations conducted throughout 200 nanoseconds, the interaction analysis of complexes PS_CID2813602 and PS_24357538 revealed the persistence of 1 hydrogen bond. In contrast, complex PS_CID753354 not only maintained 1 hydrogen bond consistently throughout the simulation duration but also displayed the formation of an additional 2 hydrogen bonds. Moreover, complex PS_CID4798023 consistently exhibited 2 hydrogen bonds during the entire simulation period. Particularly, this complex also demonstrated the transient formation of 3 hydrogen bonds specifically between frames 1500–3000 and 5500–9500. As a reference point, the control complex consistently presented 5–6 hydrogen bonds throughout the simulation as shown in Figure 5.

2.4. MM/GBSA Calculation

Molecular Mechanics/Generalized Born Surface Area (MM/GBSA) approach, binding free energies for a range of molecular complexes were precisely calculated by rigorous quantitative calculations. This complex computational method is crucial for understanding the complicated energy involved in molecular interactions, especially in the context of protein-ligand complexes. By combining different energy components including van der Waals forces, electrostatic interactions, and solvation effects-which include both polar and non-polar contributions-the MM/GBSA method calculates the binding free energy. The binding free energy of the molecular complex chosen PS_CID2813602 was found to be −53.99 Kcal/mol in this thorough assessment. This data point indicates a favourable binding interaction that is probably driven by a strong intermolecular

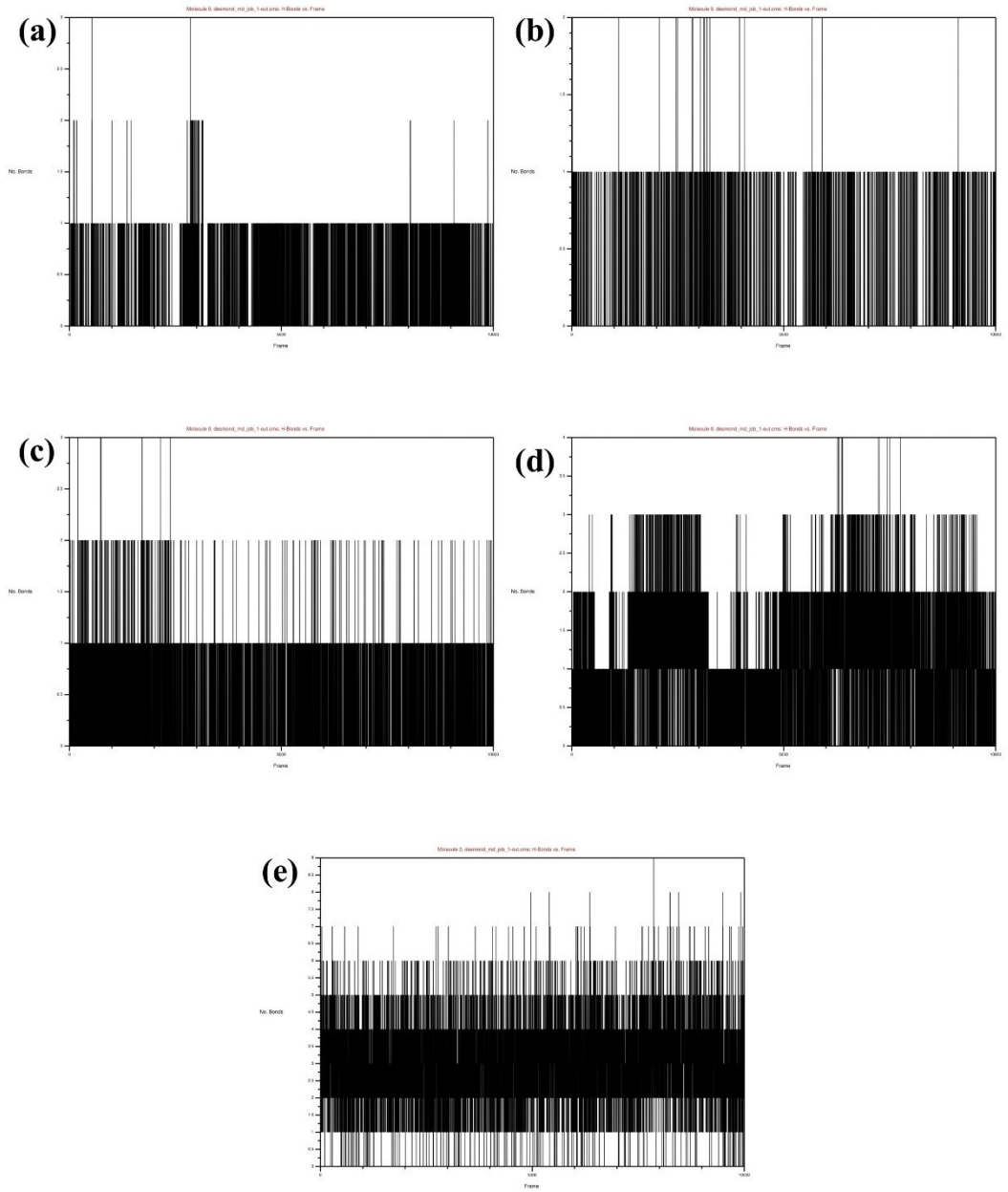

Figure 5. Hydrogen bond analysis of four selected complexes (a) PS_CID2813602, (b) PS_24357538, (c) PS_CID753354 (d) PS_CID4798023 and (e) control (PA) docked with the PS protein.

force network. In the same way, the complex PS_24357538 Gibbs free energy (ΔG) was calculated to be −55.14 Kcal/mol, indicating a similar or maybe slightly stronger affinity towards its binding partner than PS_CID2813602. On the other hand, PS_CID753354 had an entirely distinct profile, with an ΔG value of −60.43 Kcal/mol. Under usual preferences, this high ΔG value suggests a less favourable or perhaps adverse binding interaction. It might be related to reduced intermolecular pressures or harmful entropic changes upon binding. On the other hand, PS_CID4798023 had a highly strong binding affinity, as determined by its estimated ΔG of −56.95 Kcal/mol. This indicates the interactions in this complex are quite strong, with strong attractive forces and maybe the best possible geometric alignment between the binding site and the ligand. The study's control complex, which functions as a standardization level to comprehend these interactions, has an ΔG of −101.51 Kcal/mol for comparison reasons. An important point of reference for placing the binding efficiencies of the compounds under investigation in context is the much lower energy observed, which highlights a significantly greater binding affinity in the control complex. The data presented in this work and reported in Table 2 reveals these varying binding affinities, which are important insights about the molecular basis of ligand-receptor interactions and may have implications for the deliberate development of more effective therapeutics or inhibitors as mentioned in Table 2.

Table 2. MMGBSA analysis of four selected complexes (a) PS_CID2813602, (b) PS_24357538, (c) PS_CID753354 (d) PS_CID4798023 and (e) control (PA) docked with the PS protein.

Energy components/Complexes	PS_CID2813602	PS_24357538	PS_CID753354	PS_CID 4798023	PS_Control
Van der Waal energy (ΔVDWAALS)	−49.69 ± 2.76	−50.19 ± 2.44	−48.06 ± 2.11	−58.13 ± 2.22	−63.77 ± 2.62
Electrostatic energy (ΔEEL)	41.87 ± 14.55	−14.83 ± 3.50	29.81 ± 16.49	−2.83 ± 3.07	−59.53 ± 6.24
Polar solvation energy (ΔEGB)	−36.36 ± 13.66	24.01 ± 2.81	−30.66 ± 16.02	17.20 ± 1.80	34.48 ± 3.74
Non-polar solvation energy (ΔESURF)	−9.81 ± 0.85	−14.13 ± 1.30	−11.52 ± 0.66	−13.18 ± 0.63	−12.68 ± 0.71
Net gas phase energy (ΔGGAS)	−7.82 ± 17.31	−65.03 ± 5.94	−18.24 ± 18.61	−60.97 ± 5.30	−123.31 ± 4.46
Net solvation energy (ΔGSOLV)	−46.17 ± 14.52	9.88 ± 4.11	−42.18 ± 16.69	4.02 ± 2.44	21.79 ± 4.46
ΔG_{total}	−53.99 ± 31.83	−55.14 ± 10.06	−60.43 ± 35.30	−56.95 ± 7.74	−101.51 ± 13.33

2.5. Principal Component Analysis

Principal Component Analysis (PCA) is mostly employed for the dimensionality reduction of multidimensional datasets, striving to retain pivotal information. This technique is particularly useful in the context of molecular dynamics (MD) simulations for examining the dynamic stability of molecular complexes as shown in Figure 6. In this study, PCA was applied to the trajectory data of several complexes, including PS_CID2813602, PS_CID6622018, PS_CID753354, PS_CID 4798023, and a PS_PA complex to discern patterns of conformational changes and assess their stability. In the PS_CID2813602 complex, PCA generated scatter plots, particularly between frames 2000 and 6000, indicating a stable conformational state. Particularly, at frame 4000, minor alterations were observed, suggesting the presence of conformational variations and the occurrence of common conformers during the simulation. This implies that the PS_CID2813602 complex exhibited dynamic stability with periodic conformational changes. In the case of the PS_CID6622018 complex, scatter plots remained stable from frame 2000–8000, indicative of its dynamic stability. This pattern suggests that, like PS_CID2813602, PS_CID6622018 underwent conformational changes throughout the MD simulation. The analysis of the PS_CID753354 complex revealed a dense plot distribution in the range of 4000–10000 frames, consistent with a stable conformational state. This pattern denotes that PS_CID753354 also experienced conformational changes, yet maintained overall stability. Contrastingly, the PS_CID4798023 complex exhibited a dense plot indicative of negligible conformational changes, signifying a high degree of stability throughout the simulation period. Lastly, the PS_PA complex demonstrated a dense plot with minor scatterings, implying the presence of minimal conformational changes while maintaining acceptable stability.

2.6. Free Energy Landscape

In the context of molecular dynamics simulations, the free energy landscape serves as a comprehensive depiction of the energy distribution and conformational dynamics within a biomolecular system. These landscapes, as illustrated in Figure 7, provide crucial insights into the energetic implications of conformational alterations. They visually represent the dynamic conformational changes occurring during the simulation, culminating in the formation of a low-energy structure, often resembling a narrow, funnel-like configuration. Furthermore, areas of deep blue within the extensive free energy landscape denote the presence of localized energy minima, indicating periods during the simulation when the protein structures attained their lowest energy states. In the ligand-bound complexes, these local minima, depicted in dark blue, were notably pronounced, highlighting the achievement of minimal energy structures.

In Figure 7, the depicted molecular entities, specifically PS_24357538 and PS_CID 4798023, are characterized by the presence of narrow basins within the free energy landscape. These narrow basins are indicative of highly stable states. The stability is inferred from the limited energy fluctuations and a reduced frequency of conformational transitions. This implies that these molecules predominantly reside in a specific conformational state, with minimal deviation from this state, signifying a high degree of structural rigidity or a tightly regulated energy state. Such characteristics are often associated with a reduced likelihood of spontaneous conformational changes, suggesting a highly specific and possibly functionally focused state. Conversely, molecules PS_CID2813602, PS_CID753354, and PS_PA are represented with wider basins in the same free energy landscape. The wider basins suggest a greater diversity in the attainable conformational states, with a correspondingly higher frequency of transitions between these states. This implies a more dynamic structural nature for these molecules, with an increased propensity for undergoing conformational changes. The wider basins are indicative of a landscape where multiple minima exist, allowing for a variety of stable states, each corresponding to different conformations. This diversity in stable states is reflective of a system with a more versatile functional repertoire, capable of adapting to varying molecular interactions or environmental conditions. Notably, molecule PS_CID 4798023, despite being grouped with PS_24357538 in terms of exhibiting narrow basins, deserves particular attention due to its manifestation of deep energy wells within these narrow basins. This characteristic suggests an even greater stability and a more pronounced limitation in the transitional occurrences. The deep energy wells indicate that once this molecule adopts a particular conformation, it is

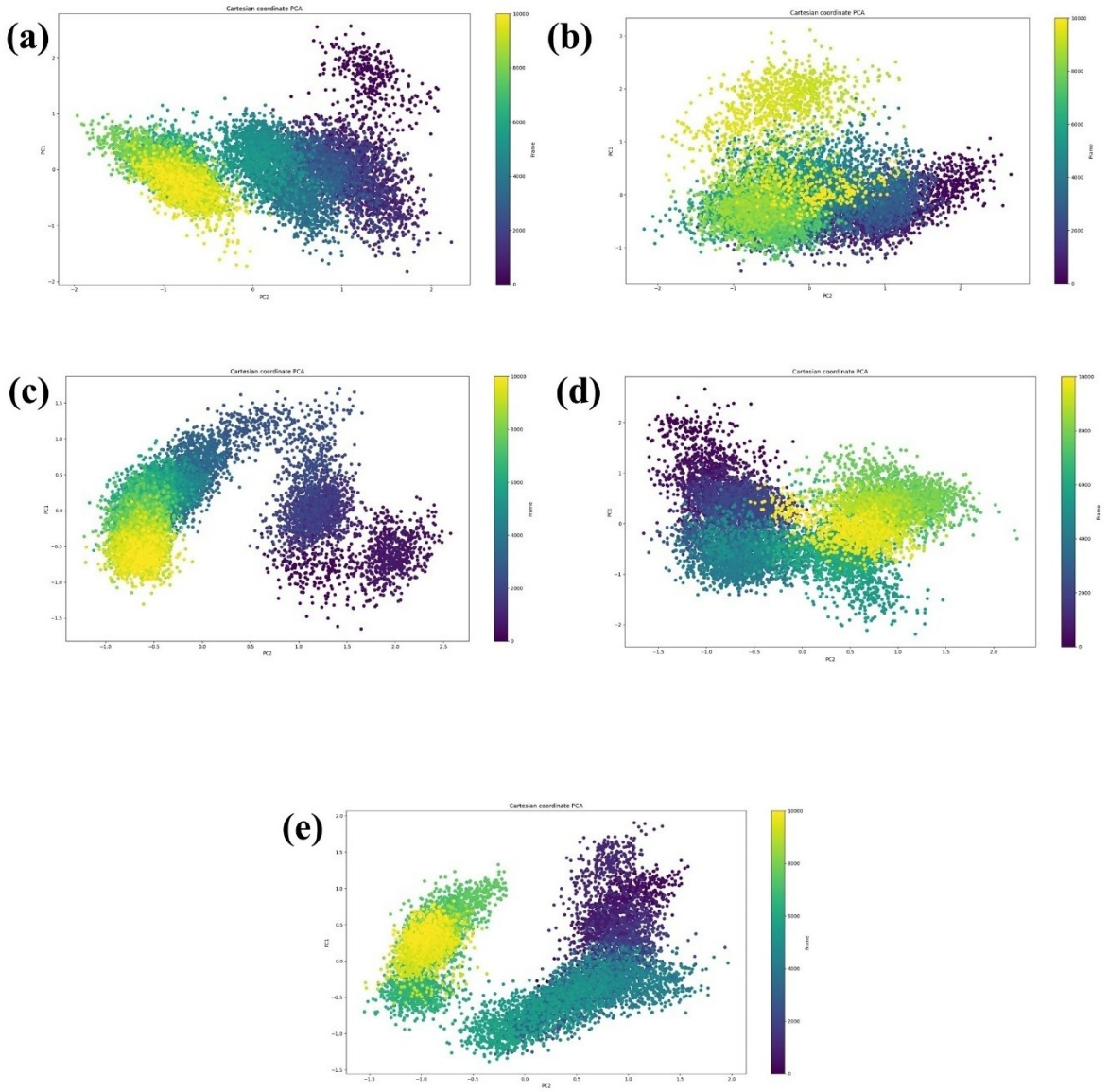

Figure 6. PCA analysis of four selected complexes (a) PS_CID2813602, (b) PS_24357538, (c) PS_CID753354 (d) PS_CID4798023 and (e) control (PA) docked with the PS protein.

energetically unfavorable for it to transition out of this state. This could be due to a particularly favorable interaction within the molecular structure or with a ligand, which stabilizes this conformation. Such a feature is significant as it may imply a highly specific functional role for PS_CID 4798023, where the molecule is optimized for a particular interaction or activity, with minimal deviation from this optimized state.

It is noteworthy that the minimal energy state, which acts as the point of reference, was consistently determined to be 0 kJ/mol for all the complexes. The relative maximum energy state ranged from 12 kJ/mol–14 kJ/mol. Moreover, it is important to mention that all complexes have a stable conformation as long as the energy threshold stays below 2 kJ/mol. The stable conformation is shown by a dark blue hue in Figure 7. This state of low energy indicates a considerable level of stability and a reduced likelihood of undergoing conformational changes under typical circumstances. In the context of molecular dynamics simulations, it is crucial as it identifies the areas of the energy landscape where the complexes are more probable to occur during their normal functioning. The discovery of four minimal energy poses is a vital feature for each complex, which was retrieved from the lower energy state. These poses depict the most stable configurations that the complex may assume. The superimposition of these poses with their initial pose was created, as seen in Figure 8, offering a visual and quantitative picture of the stability and conformational changes observed over the 200 ns simulation period. Visual and quantitative comparison of the initial and end states of the complexes is a critical stage in molecular dynamics investigations. This phase provides valuable insights into the dynamic behaviors and potential functional implications of the complexes in their natural settings. We computed the collective

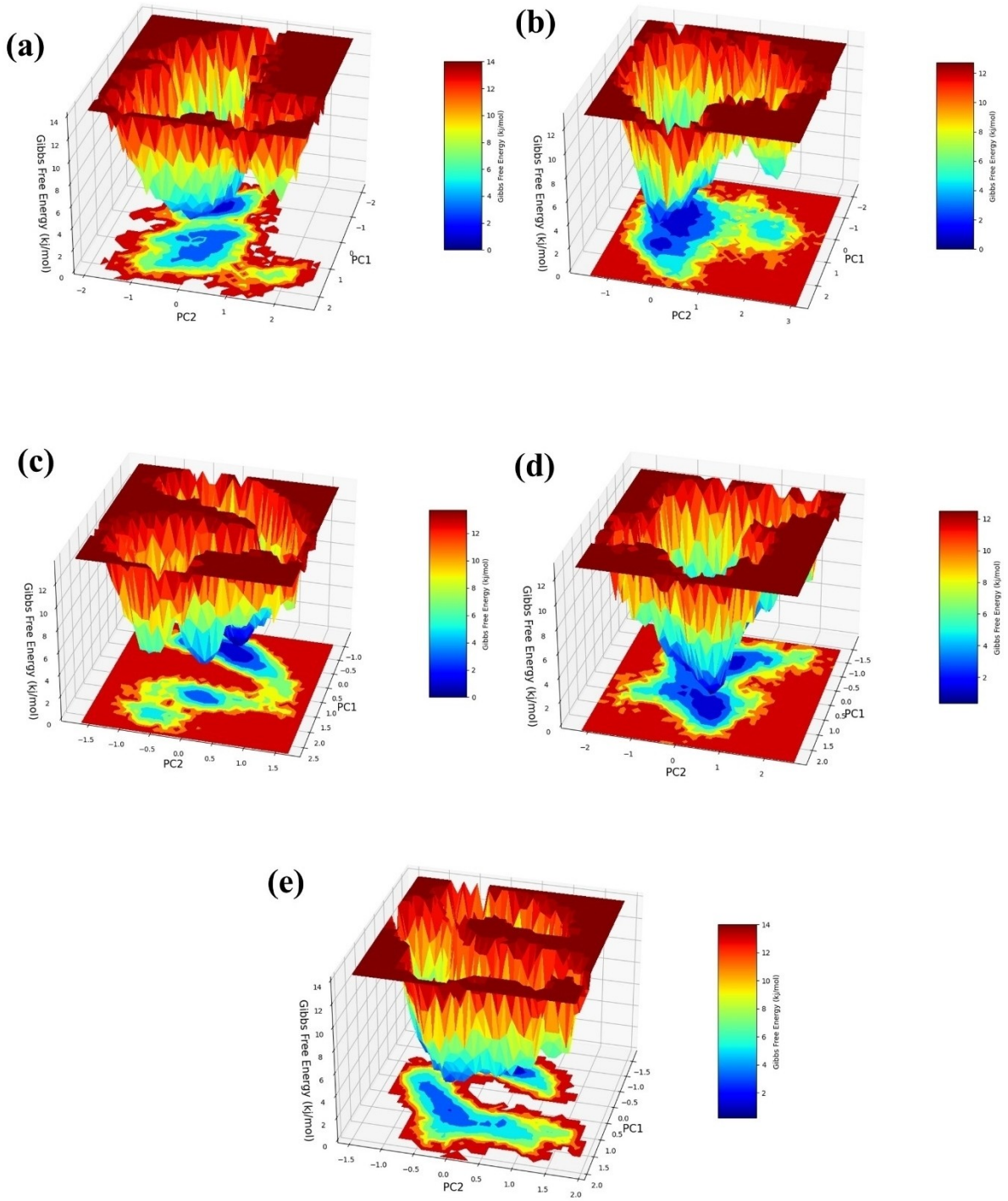

Figure 7. FEL analysis of four selected complexes (a) PS_CID2813602, (b) PS_24357538, (c) PS_CID753354 (d) PS_CID4798023 and (e) control (PA) docked with the PS protein.

root mean square deviation (RMSD) of these aligned positions. The RMSD computation yields information on the extent to which these poses differ from a reference structure, offering valuable insights into the complex's flexibility and structural changes.

The protein complex PS_CID2813602 demonstrated an RMSD overall RMSD value of 1.324 angstroms (Å), indicating a moderate structural deviation from the reference model. This suggests some conformational changes, possibly due to factors like ligand binding or mutations, but not extensive alterations. The complex PS_24357538, with an overall RMSD of 1.271 Å, shows a closer alignment to the reference, implying a more conserved structure or higher stability under similar conditions.

Conversely, PS_CID753354 exhibited an overall RMSD of 1.374 Å, a value pointing to greater structural deviations. This could be reflective of substantial conformational changes,

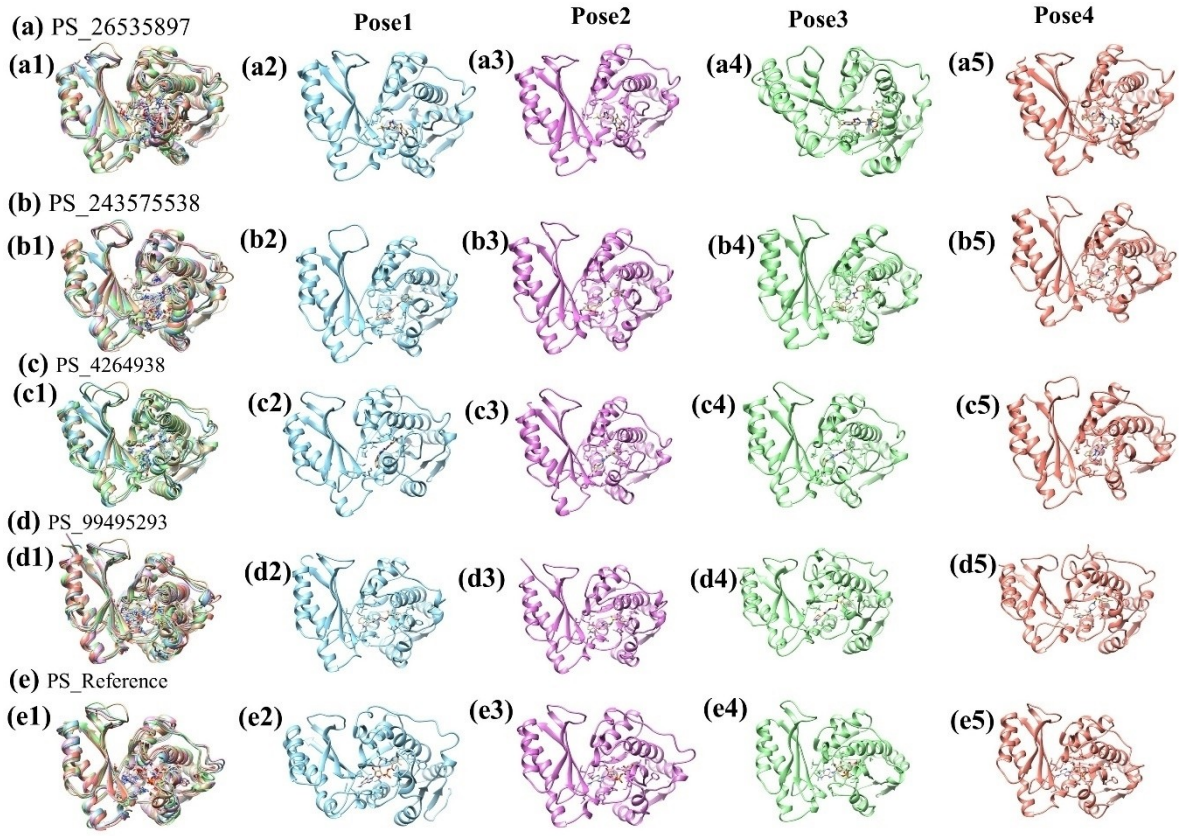

Figure 8. This graph shows the superimposition that was taken from the state with the lowest energy, i. e. (a) PS_CID2813602, (b) PS_24357538, (c) PS_CID753354, and (d) PS_CID 4798023. (e) Reference Compound Complex PA. It is divided into five parts: (a1, a2, a3, a4), (b1, b2, b3, b4), (c1, c2, c3, c4), (d1, d2, d3, d4), and (e1, e2, e3, e4). Panel (a1, b1, c1, d1, and e1) depicts the arrangement of (a2, a3, a4), (b2, b3, b4), (c2, c3, c4), (d2, d3, d4), and (e2, e3, e4) reflecting the lowest energy state.

possibly due to varied protein interactions or environmental factors. The most significant deviation was observed in PS_CID 4798023, with an overall RMSD of 1.477 Å. This high RMSD might indicate major structural differences, crucial for understanding this protein's functional aspects, possibly arising from extensive conformational changes or alternative folding patterns. The control complex, analyzed for comparative purposes, showed an overall RMSD of 1.288 Å. This serves as a benchmark, providing a baseline to contextualize the structural variations observed in the experimental complexes. These RMSD values reveal the structural dynamics of these protein complexes, shedding light on how various factors impact their 3D conformations. Such understanding is key in fields like drug design, protein engineering, and the study of molecular mechanisms underlying diseases.

3. Discussion

In discussing the identified compounds and their complexes with Pantothenate Synthetase in *Mycobacterium tuberculosis*, it's vital to delve into the specific interactions and implications of these findings for TB drug development. The compounds, CID2813602, 24357538, CID753354, and CID 4798023, exhibited notable binding affinities, highlighting their potential as inhibitors of the enzyme. Additionally, the reference molecule Pantoyl Adenylate (PA) was used to benchmark these interactions. The pantothenate synthetase as a noval target was also reported in similar research conducted by Pradhan and his colleague.[25] CID2813602 compound showed a binding energy of −10.9 kcal/mol, indicating a strong interaction with the active site of Pantothenate Synthetase. The formation of a complex with the enzyme suggests that CID2813602 could effectively inhibit the enzymatic activity necessary for coenzyme A biosynthesis. Its interaction might involve hydrogen bonding and hydrophobic interactions, contributing to its high affinity and potential specificity as an inhibitor. Compound 24357538 With a binding energy of −11.4 kcal/mol, 24357538 represents one of the most promising candidates for inhibiting Pantothenate Synthetase. The complex formed by this compound and the enzyme likely disrupts the enzyme's natural substrate binding, inhibiting its function. Analyzing the precise interactions-such as key amino acid residues involved in binding-can provide insights into its mechanism of action and guide the optimization of its inhibitory activity.[37] The compound CID753354, exhibited a binding energy of −11.3 kcal/mol, which suggests another strong candidate for enzyme inhibition. The specific interactions that facilitate this binding energy-potentially including both electrostatic and van der Waals interactions-underscore the compound's potential efficacy. Understanding

the complex formed between CID753354 and Pantothenate Synthetase can reveal critical insights into the structural requirements for effective inhibition.

Compound CID4798023 exhibited a binding energy of −10.2 kcal/mol, CID 4798023, while having a slightly higher binding energy than the others, still holds promise as a potential inhibitor. The compound-enzyme complex analysis can identify the molecular determinants of binding affinity, providing a basis for structural modifications to enhance inhibitory activity.[40] The inclusion of Pantoyl Adenylate (PA) as a reference molecule is crucial for benchmarking the effectiveness and specificity of the identified compounds. PA's interaction with Pantothenate Synthetase provides a comparative baseline to assess the binding energies and inhibitory potentials of the novel compounds. Understanding the binding mode and affinity of PA can also offer insights into the structural features important for effective inhibition, guiding the design of more potent inhibitors.[31] The identification of these compounds and their complexes with Pantothenate Synthetase highlights the potential for developing novel anti-TB drugs targeting a critical enzymatic pathway in *M. tuberculosis*. These findings underscore the importance of targeting enzyme functions essential for bacterial survival, offering a strategic approach to combat drug resistance. Future research should focus on experimental validation of these compounds' inhibitory effects, detailed mechanistic studies of their interactions with Pantothenate Synthetase, and optimization for improved pharmacokinetic and pharmacodynamic properties. Additionally, exploring the structural diversity among these compounds can aid in the development of a robust pipeline of potential anti-TB agents, addressing the urgent need for new therapies against drug-resistant forms of tuberculosis.

4. Conclusions

This study represents a pivotal advancement in the fight against tuberculosis a global health challenge exacerbated by the emergence of drug-resistant strains of *Mycobacterium tuberculosis*. Our research utilized computational drug discovery methods to identify four potential inhibitors, namely CID2813602, CID24357538, CID753354, and CID4798023, targeting Pantothenate Synthetase, an enzyme critical for the bacterium's survival. These compounds demonstrated strong binding energies and significant interactions, including hydrogen bonds, suggesting their strong binding affinity with the target protein. The ADMET analysis of these compounds reveals several promising attributes across their pharmacokinetic and safety profiles, indicating strong potential for further development and optimization. CID2813602 exhibits moderate absorption and distribution, effective systemic circulation, and high plasma protein binding (PPB), contributing to prolonged therapeutic effects. Its interactions with CYP enzymes offer opportunities for fine-tuning to enhance bioavailability. Despite lower solubility and permeability, CID24357538 shows significant CYP enzyme interactions, which can be strategically modified to improve absorption and therapeutic efficacy. CID753354 stands out with excellent absorption and an extended half-life, which makes it ideal for sustained therapeutic action and reduces the need for frequent dosing. CID4798023 is notable for its exceptional blood-brain barrier penetration, making it a strong candidate for central nervous system applications, with its high clearance rate ensuring efficient elimination and reduced toxicity. The control compound exhibits a well-balanced ADMET profile, with low CYP interactions, good solubility, and reduced carcinogenic potential, suggesting a lower risk of adverse interactions and a favorable safety profile. These findings highlight the unique strengths of each compound, demonstrating their potential for therapeutic development. The trajectory analysis of each compound from the MD simulation exhibited promising results. The RMSD and RMSF analysis confirmed the global and local stability of each complex compared to the reference compound Pantoyl Adenylate. The PCA-based Free Energy Landscape analysis showed the presence of minimum energy regions with narrow basins in most complexes, suggesting stable nature due to global minima. The free binding energy obtained through MM/GBSA calculation indicated significant contributions to binding stability. These findings suggest that these selected compounds have the potential to inhibit the target protein essential for pathogen survival, forming the foundation for new anti-TB agents. Additionally, this study underscores the potential of computational drug discovery in accelerating the identification of new therapeutic targets, offering hope for more effective treatments against TB and other infectious diseases.

Acknowledgments

The authors extend their appreciation to the Deanship of Scientific research at Northern Border University, Arar, KSA for funding this research work through the project number " NBU-FFR-2024–2043–06".

Conflict of Interests

The authors declare no conflict of interest.

Data Availability Statement

The data that support the findings of this study are available on request from the corresponding author. The data are not publicly available due to privacy or ethical restrictions.

Keywords: *Mycobacterium tuberculosis* · MD simulation · Hydrogen bond analysis · PCA

[1] R. Baptista, S. Bhowmick, J. Shen, L. A. J. Mur, *Molecules* **2021**, *26*, 475, https://doi.org/10.3390/molecules26020475.
[2] H. M. Berman, J. Westbrook, Z. Feng, G. Gilliland, T. N. Bhat, H. Weissig, I. N. Shindyalov, P. E. Bourne, *Nucleic Acids Res.* **2000**, *28*, 235–242.

[3] H. S. Butman, T. J. Kotzé, C. S. Dowd, E. Strauss, *Front. Cell Infect. Microbiol.* **2020**, *10*, 605662, https://doi.org/10.3389/fcimb.2020.605662.
[4] D. A. Case, H. M. Aktulga, K. Belfon, D. S. Cerutti, G. A. Cisneros, V. W. D. Cruzeiro, N. Forouzesh, T. J. Giese, A. W. Götz, H. Gohlke, S. Izadi, K. Kasavajhala, M. C. Kaymak, E. King, T. Kurtzman, T.-S. Lee, P. Li, J. Liu, T. Luchko, R. Luo, M. Manathunga, M. R. Machado, H. M. Nguyen, K. A. O'Hearn, A. V. Onufriev, F. Pan, S. Pantano, R. Qi, A. Rahnamoun, A. Risheh, S. Schott-Verdugo, A. Shajan, J. Swails, J. Wang, H. Wei, X. Wu, Y. Wu, S. Zhang, S. Zhao, Q. Zhu, T. E. I. Cheatham, D. R. Roe, A. Roitberg, C. Simmerling, D. M. York, M. C. Nagan, K. M. Merz Jr., *J. Chem. Inf. Model.* **2023**, *63*, 6183–6191, https://doi.org/10.1021/acs.jcim.3c01153.
[5] D. A. Case, T. E. Cheatham, T. Darden, H. Gohlke, R. Luo, K. M. Merz, A. Onufriev, C. Simmerling, B. Wang, R. J. Woods, *J. Comput. Chem.* **2005**, *26*, 1668–1688, https://doi.org/10.1002/jcc.20290.
[6] Chiacchiaretta M. 2022. M. tuberculosis lineages: genetic diversity and its involvement on macrophage infection and on drug tolerance. Doctoral Thesis. https://dx.doi.org/10.25434/chiacchiaretta-matteo_phd2022.
[7] A. Czumaj, S. Szrok-Jurga, A. Hebanowska, J. Turyn, J. Swierczynski, T. Sledzinski, E. Stelmanska, *Int. J. Mol. Sci.* **2020**, *21*, 9057, https://doi.org/10.3390/ijms21239057.
[8] W. L. DeLano, *CCP4 Newsl. Protein Crystallogr.* **2002**, *40*, 82–92.
[9] J. Eberhardt, D. Santos-Martins, A. F. Tillack, S. Forli, *J. Chem. Inf. Model.* **2021**, *61*, 3891–3898.
[10] M. Hassam, K. Khan, K. Jalal, M. Tariq, S. Tarique Moin, R. Uddin, *J. Biomol. Struct. Dyn.* **2023**, 1–18. https://doi.org/10.1080/07391102.2023.2260483.
[11] F. Huang, Y. Zhao, *Zoonoses* **2022**, *2*, e991. https://doi.org/10.15212/ZOONOSES-2021-0021.
[12] J. P. Hughes, S. Rees, S. B. Kalindjian, K. L. Philpott, *Br. J. Pharmacol.* **2011**, *162*, 1239–1249.
[13] W. Humphrey, A. Dalke, K. Schulten, *J. Mol. Graph* **1996**, *14*, 33–38, 27–28, https://doi.org/10.1016/0263–7855(96)00018–5.
[14] N. Jaiswal, A. Kumar, *Bioinform. Adv.* **2023**, *3*, vbad090, https://doi.org/10.1093/bioadv/vbad090.
[15] L. P. Kagami, G. M. das Neves, L. F. S. M. Timmers, R. A. Caceres, V. L. Eifler-Lima, *Comp. Biol. Chem.* **2020**, *87*, 107322.
[16] J. L. Khawbung, D. Nath, S. Chakraborty, *Comp. Immunol. Microbial. Infect. Dis.* **2021**, *74*, 101574.
[17] C. M. Labbé, J. Rey, D. Lagorce, M. Vavruša, J. Becot, O. Sperandio, B. O. Villoutreix, P. Tufféry, M. A. Miteva, *Nucleic Acids Res* **2015**, *43*, W448–W454, https://doi.org/10.1093/nar/gkv306.
[18] M. Hassam, J. A. Shamsi, A. Khan, A. Al-Harrasi, R. Uddin, *Computers in Biology and Medicine* **2022**, *145*, 105453. https://doi.org/10.1016/j.compbiomed.2022.105453.
[19] P. Mark, L. Nilsson, *J. Phys. Chem. A* **2001**, *105*, 9954–9960.
[20] B. R. Miller, T. D. McGee, J. M. Swails, N. Homeyer, H. Gohlke, A. E. Roitberg, *J. Chem. Theory Comput.* **2012**, *8*, 3314–3321, https://doi.org/10.1021/ct300418h.
[21] D. M. Morens, A. S. Fauci, *PLoS Pathog.* **2013**, *9*, e1003467.
[22] MTiOpenScreen [WWW Document] **n.d.**, https://bioserv.rpbs.univ-paris-diderot.fr/services/MTiOpenScreen/ (accessed: 19 January 2024).
[23] H. G. Petersen, *J. Chem. Phys.* **1995**, *103*, 3668–3679, https://doi.org/10.1063/1.470043.
[24] E. F. Pettersen, T. D. Goddard, C. C. Huang, G. S. Couch, D. M. Greenblatt, E. C. Meng, T. E. Ferrin, *J. Comput. Chem.* **2004**, *25*, 1605–1612.
[25] S. Pradhan, C. Sinha, *In Silico Pharmacol.* **2018**, *6*, 9, https://doi.org/10.1007/s40203–018–0046–4.
[26] S. Ravimohan, H. Kornfeld, D. Weissman, G. P. Bisson, *Eur. Respir. Rev.* **2018**, *27*, 170077. doi: 10.1183/16000617.0077-2017.
[27] J.-P. Ryckaert, G. Ciccotti, H. J. C. Berendsen, *J. Comput. Phys.* **1977**, *23*, 327–341, https://doi.org/10.1016/0021–9991(77)90098–5.
[28] D. Studio, Discovery studio. Accelrys [2.1] **2008**, BIOVIA, Dassault Systèmes (2020). Discovery Studio Visualizer, San Diego, CA, USA.
[29] A. Suresh, S. Srinivasarao, Y. M. Khetmalis, S. Nizalapur, M. Sankaranarayanan, K. V. G. C. Sekhar, *RSC Adv.* **2020**, *10*, 37098–37115.
[30] W. L. DeLano, *Newsl. Protein Crystallogr* **2002**, *40*, 82–92.
[31] V. C. C. Uy, J. B. Billones, *Phil. Sci. Lett.* **2012**, *5*, 122–130.
[32] H. Verma, A. Chauhan, A. Kumar, M. Kumar, K. Kanchan, *Life Sci.* **2024**, *346*, 122632, https://doi.org/10.1016/j.lfs.2024.122632.
[33] J. Wang, W. Wang, P. A. Kollman, D. A. Case, *J. Mol. Graphics Modell.* **2006**, *25*, 247–260.
[34] J. Wang, R. M. Wolf, J. W. Caldwell, P. A. Kollman, D. A. Case, *J. Comput. Chem.* **2004**, *25*, 1157–1174.
[35] S. Wang, D. Eisenberg, *Protein Sci.* **2003**a, *12*, 1097–1108.
[36] S. Wang, D. Eisenberg, *Protein Sci.* **2003**b, *12*, 1097–1108.
[37] E. L. White, K. Southworth, L. Ross, S. Cooley, R. B. Gill, M. I. Sosa, A. Manouvakhova, L. Rasmussen, C. Goulding, D. Eisenberg, *J. Biomol. Screening* **2007**, *12*, 100–105.
[38] F. Wu, Y. Zhou, L. Li, X. Shen, G. Chen, X. Wang, X. Liang, M. Tan, Z. Huang, *Front. Chem.* **2020**, *8*, 726.
[39] W. Yan, Y. Zheng, C. Dou, G. Zhang, T. Arnaout, W. Cheng, *Mol. Biomed.* **2022**, *3*, 48.
[40] Y. Yang, P. Gao, Y. Liu, X. Ji, M. Gan, Y. Guan, X. Hao, Z. Li, C. Xiao, *Bioorg. Med. Chem. Lett.* **2011**, *21*, 3943–3946.

Manuscript received: May 1, 2024